ACS OMEGA

http://pubs.acs.org/journal/acsodf Article

A Single-Component Molecular Glass Resist Based on Tetraphenylsilane Derivatives for Electron Beam Lithography

Yake Wang, Jundi Yuan, Jinping Chen,* Yi Zeng, Tianjun Yu, Xudong Guo, Shuangqing Wang, Guoqiang Yang,* and Yi Li*

Cite This: *ACS Omega* 2023, 8, 12173−12182

Read Online

ACCESS | Metrics & More | Article Recommendations | Supporting Information

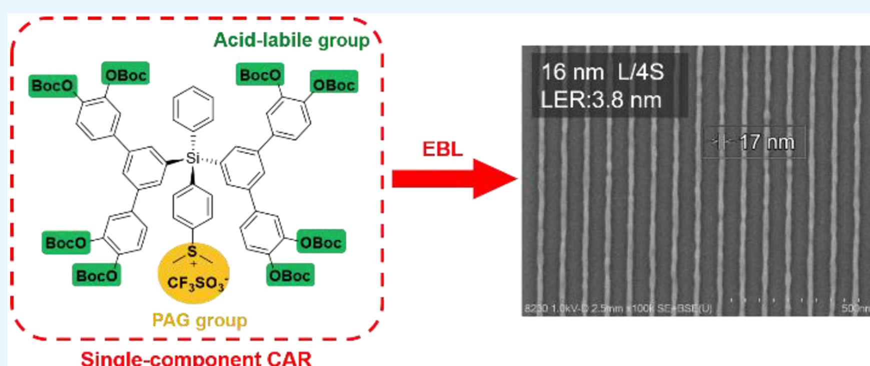

ABSTRACT: A novel molecular glass (TPSiS) with photoacid generator (sulfonium salt group) binding to tetraphenylsilane derivatives was synthesized and characterized. The physical properties such as solubility, film-forming ability, and thermal stability of TPSiS were examined to assess the suitability for application as a candidate for photoresist materials. The sulfonium salt unit underwent photolysis to effectively generate photoacid on UV irradiation, which catalyzed the deprotection of the *t*-butyloxycarbonyl groups. It demonstrates that the TPSiS can be used as a 'single-component' molecular resist without any additives. The lithographic performance of the TPSiS resist was evaluated by electron beam lithography. The TPSiS resist can resolve 25 nm dense line/space patterns and 16 nm L/4S semidense line/space patterns at a dose of 45 and 85 $\mu C/cm^2$ for negative-tone development (NTD). The etching selectivity of the TPSiS resist to Si substrate is 8.6 under SF_6/O_2 plasma, indicating a potential application. Contrast analysis suggests that the significant solubility switch within a narrow exposure dose range (18−47 $\mu C/cm^2$) by NTD is favorable for high-resolution patterns. This study supplies useful guidelines for the optimization and development of single-component molecular glass resists with high lithographic performance.

■ INTRODUCTION

The fabrication of nanoscale semiconductor devices increasingly requires high-resolution patterns with smaller feature sizes to meet expectations set by Moore's law.[1−4] As the feature size decreases, the requirements for resists' performance have gradually increased. Chemically amplified resists (CARs) have dominated the semiconductor industry for decades due to their high sensitivity.[5−7] Usually, CARs are mainly composed of organic matrix resins, photoacid generators (PAGs), and other additives. The ratio of PAG is generally very low and leads to the sparse spatial distribution of PAG in resist films, which may cause serious stochastic effects. The stochastic distribution of PAGs and the uncontrolled diffusion of acid in the resist film result in poor line edge roughness (LER), suggesting a resolution limit for CARs. Although a high loading ratio of PAG is beneficial to decreasing the stochastic effects, it would result in other problems including microphase separation,[8] inhomogeneity distribution due to self-aggregation.[9,10] The PAGs tend to avoid or seek the resist-air[11] or resist-substrate interfaces.[12] Besides, the plasticization effect of blended PAG will decrease the glass-transition temperature (T_g) of the resist film.[13] These intrinsic problems may lead to a worse LER and negatively affect the ultimate resolution of resist patterns.

One approach to solving the limitation of resolution is the development of nonchemically amplified resists (n-CARs). Some novel n-CARs based on polycarbonates,[14] metal-containing clusters,[15−17] metal−organic complexes,[18−21] polymer containing sulfonium salt,[22,23] have been investigated to

Received: December 21, 2022
Accepted: February 21, 2023
Published: March 21, 2023

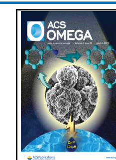

© 2023 The Authors. Published by American Chemical Society

achieve sub-20 nm patterning under e-beam exposure. Although the resolution has been greatly increased, the sensitivity still needs to be further improved. Another effective approach to overcoming these limitations in CARs is to covalently link the PAG to the resist material, of which the PAG units are incorporated into polymer side chains.[24−31] The PAG-bound polymer acts as a 'single-component' resist and exhibits improved lithographic performances, such as short acid diffusion,[25,32−35] high contrast[24] and sensitivity.[24,25,32,34,36] The other potential advantages of the single-component resist have also been confirmed, such as restraint of pattern blur,[32] less swelling of patterns,[34,37] high etching resistance,[38] and suppression of top loss.[35] Therefore, the strategy of the PAG-bound single-component is considered an effective approach to improving the overall performance.

Molecular glasses (MGs) are a new type of low molecular weight organic compounds with well-defined structures and functional groups. They are a promising alternative to conventional polymer resists in CAR systems because monodisperse building blocks and magnitude smaller in size than polymers are beneficial for achieving high-resolution patterns with lower LER.[39−43] Combined with the concept of single-component polymer resists, PAG-bound MG resists are expected to break through the resolution-LER-sensitivity trade-off. Up to now, only a few examples of PAG-bound MG resists have been reported,[44−47] exhibiting an improved LER (3.9 nm) and resolution (24 nm HP).[45,46] Ionic sulfonium salts are usually selected as PAG-binding groups due to their high thermal stability and photoacid generating efficiency. However, most of them suffer from a significant dark loss because of the intrinsic solubility of the ionic compounds in aqueous developer, which limits the pattern resolution by positive-tone development (PTD).[47]

Tetraphenylsilane (TPSi) has a branched and nonplanar structure, which enables the formation of amorphous films. The modification of TPSi is facile.[48,49] Our recent research has demonstrated that MG resists based on TPSi derivatives exhibit excellent thermal stability, film-forming ability, and high-resolution pattern performances.[49] Further, a new strategy of dual-tone developed molecular resists was proposed in our report, demonstrating a promising method to improve overall lithographic performance.[50] As a continuation, a novel PAG-bound MG (TPSiS) was designed and prepared by modifying TPSi with eight *t*-butyloxycarbonyl (*t*-Boc) groups and one sulfonium salt unit (Figure 1). The sulfonium salt unit is introduced into the branch chain as a photoacid generator, and the *t*-Boc groups are used to achieve solubility switch before and after exposure. The TPSiS resist combines both the benefits of MG resists with those of PAG-bound polymer resists. It is a really single-component chemically amplified molecular resist without any physically blended additives. Although the TPSiS is still ionic, which may limit the resolution of PTD, the dual-tone strategy for molecular resists may avoid the disadvantage. The TPSiS resist is anticipated to achieve high performance and is comprehensively evaluated by using electron beam lithography (EBL), demonstrating a better patterning capability by negative-tone development (NTD) than PTD.

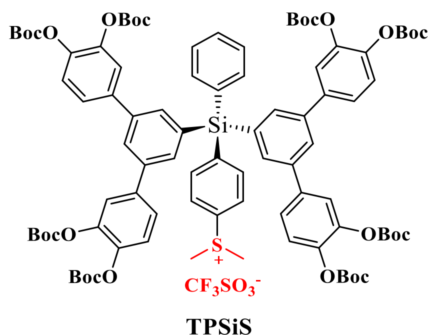

Figure 1. Structure of TPSiS molecule.

■ EXPERIMENTAL SECTION

Materials and Instruments. Ether was distilled under normal pressure. Other standard reagents and chemicals were purchased from commercial sources and used without any further purification unless otherwise noted. The electron beam resist of PMMA 950 K was purchased from KAYAKU. Nuclear magnetic resonance (NMR) spectra were measured on an Avance ∏-400 (Bruker, Germany) by dissolving samples in corresponding deuterated solvents. Thermal gravimetric (TG) was recorded on a JCT-1 (Hengjiu, China). Differential scanning calorimetry (DSC) was performed on DSC 4000 (PerkinElmer, USA) instrument at the heating rate of 10 °C min^{-1} under a nitrogen atmosphere. High-resolution mass spectroscopy (HR-MS) was performed on a Solarix FT-ICR mass spectrometer (Bruker, Germany). Powder X-ray diffraction (PXRD) traces were obtained using a D8 focus XRD (Bruker, Germany) to examine the crystallinity of the bulk material. Fourier transform infrared (FT-IR) spectra were recorded by an Excalibur 3100 IR (Varian, USA). UV−vis absorption spectra were acquired on a UV-2550 spectrophotometer (Shimadzu, Japan). Resist films were prepared by spin-coating with a CEE200X coating machine (Brewer Science CEE, USA). Resist film thickness was measured using an AST SE200BM spectroscopic ellipsometer (Angstrom Sun, USA). The photolysis properties were evaluated under exposure to a Hg lamp (254 nm) with an optical intensity (I_0) of 2.87 mW/cm^2. EB exposure experiments were performed on a Vistec EBPG 5000plus ES (Vistec, USA) at an acceleration voltage of 100 kV. Top-view and cross-sectional scanning electron microscope (SEM) images were taken by S4800 or Regulus 8230 scanning electron microscope (Hitachi, Japan). Atomic force microscope (AFM) images were taken by a Dimension FastscanBio system (Bruker, USA). The line width and line-edge roughness (LER) were measured by analyzing SEM images with ProSEM software. The etching step was performed on a plasma etching machine (Sentech/Etchlab 200, Germany) after the patterning process.

Synthesis and Characterization of TPSiS. *Compound 2.* *n*-Butyllithium (2.5 M in *n*-hexane, 8.7 mL, 21.7 mmol) was added dropwise to a dry ether solution (30 mL) containing 4-bromothioanisole (4.0 g, 19.7 mmol) under nitrogen atmosphere at 0 °C. The reaction solution was further stirred for 1 h. Phenyltrichlorosilane (3.2 mL, 19.7 mmol) was then added dropwise to the solution. The mixture was stirred and gradually allowed to warm up to room temperature for 3 h (solution A). At the same time, to a stirred solution of 1,3,5-tribromobemzene (12.4 g, 39.4 mmol) in dry ether (240 mL) was added 2.5 M *n*-butyllithium solution in hexane (15.8 mL, 39.4 mmol) dropwise at −78 °C (solution B). After stirring at −78 °C for 2 h, solution A was added dropwise into solution B. The mixture was warmed to room temperature and stirred for an additional 5 h, and the reaction was quenched with water

Scheme 1. Synthesis of the TPSiS Molecule

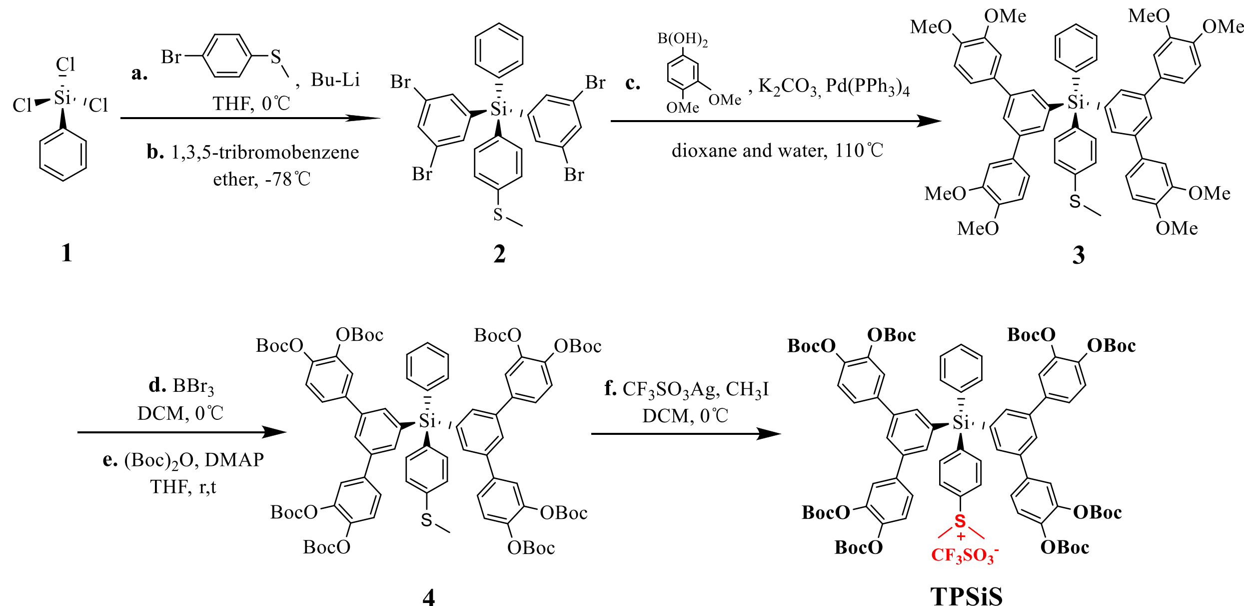

(200 mL) and extracted with ether. The product was isolated by flash column chromatography (silica gel, petroleum ether as eluent) as a white solid. Yield: 38% (5.2 g). ^{1}H NMR (400 MHz, $CDCl_3$): δ 7.77 (t, J = 1.7 Hz, 2H), 7.51 (d, J = 1.7 Hz, 4H), 7.49−7.41 (m, 5H), 7.37 (d, J = 8.2 Hz, 2H), 7.29 (d, J = 8.2 Hz, 2H), 2.51 (s, 3H). HRMS (EI): calcd for $C_{25}H_{18}Br_4SSi^+$ ([M$^+$]) 697.7591, found 697.7607.

Compound **3**. Compound **2** (4 g, 5.7 mmol), 3,4-dimethoxylphenlboronic acid (7.3 g, 40 mmol), and K_2CO_3 (5.5 g, 40 mmol) were dissolved in 1,4-dioxane (50 mL) and water (25 mL). Tetrakis(triphenylphosphine) palladium (132 mg, 0.11 mmol) was added to the solution under nitrogen atmosphere. The resulting mixture was stirred for 8 h at refluxing in nitrogen atmosphere. The mixture was cooled down to room temperature and extracted with dichloromethane. The organic phase was washed with water and dried. The solvent was removed, and the crude product was purified by flash column chromatography (silica gel, petroleum ether/ethyl acetate, 3:1). The product was isolated as a white foamy solid. Yield: 87% (4.6 g). ^{1}H NMR (400 MHz, $CDCl_3$): δ 7.78 (s, 6H), 7.71 (d, J = 6.8 Hz, 2H), 7.61 (d, J = 6.7 Hz, 2H), 7.48−7.37 (m, 3H), 7.27 (d, J = 8.7 Hz, 2H), 7.13 (d, J = 8.2 Hz, 4H), 7.04 (s, 4H), 6.92 (d, J = 8.1 Hz, 4H), 3.90 (s, 12H), 3.82 (s, 12H), 2.48 (s, 3H). HRMS (ESI): calcd for $C_{57}H_{54}NaO_8SSi^+$ ([M + Na$^+$]) 949.3201, found 949.3199.

Compound **4**. To a stirred solution of compound **3** (3.4 g, 3.7 mmol) in dry dichloromethane (35 mL) was added 0.8 M boron tribromide (BBr_3) solution in dichloromethane (25 mL, 20.8 mmol) at 0 °C. The reaction was warmed to room temperature over 2 h, quenched with water (3 mL) at 0 °C. The white precipitate was extracted with ethyl acetate. The organic phase was washed with water and dried. The solvent was removed, and the resulting residue was used directly in the next step without any purification. To a stirred solution of the above crude residue in tetrahydrofuran (THF) (30 mL) was added di-*tert*-butyl decarbonate (Boc_2O) (8.0 g, 36.7 mmol) and 4-dimethylaminopyridine (DMAP) (45 mg, 0.37 mmol) at room temperature. After stirring for 2 h, the mixture was extracted with dichloromethane. The organic extracts were washed with a dilute hydrochloric acid aqueous solution (pH = 5). The crude product was purified by flash column chromatography (silica gel, petroleum ether/ethyl acetate, 10:1). The product was isolated as a white foamy solid. Yield: 55% (3.3 g). ^{1}H NMR (400 MHz, $CDCl_3$): δ 7.74 (s, 6H), 7.62 (d, J = 7.7 Hz, 2H), 7.53 (d, J = 8.2 Hz, 2H), 7.42 (s, 4H), 7.46−7.41 (m, 3H), 7.37 (d, J = 8.4 Hz, 4H), 7.30 (d, J = 8.4 Hz, 4H), 7.29 (d, J = 8.2 Hz, 2H), 2.50 (s, 3H), 1.55 (s, 36H), 1.54 (s, 36H). HRMS (ESI): calcd for $C_{89}H_{102}Na_2O_{24}SSi_2^{2+}$ ([M + 2Na$^+$]) 830.8034, found 830.8031.

TPSiS. To a stirred solution of **4** (500 mg, 0.31 mmol) and CF_3SO_3Ag (119 mg, 0.46 mmol) in dichloromethane (5 mL) was added 0.05 M CH_3I solution in dichloromethane (10 mL, 0.46 mmol) dropwise at 0 °C. After stirring at 0 °C for 30 min, the reaction was purified by flash column chromatography (silica gel, dichloromethane/methanol, 10:1). The product was isolated as a yellow foamy solid. Yield: 64% (350 mg). ^{1}H NMR (400 MHz, $CDCl_3$): δ 7.94 (d, J = 8.1 Hz, 2H), 7.87 (d, J = 8.1 Hz, 2H), 7.79 (s, 2H), 7.66 (s, 4H), 7.61 (d, J = 6.7 Hz, 2H), 7.56−7.47 (m, 3H), 7.41 (s, 4H), 7.37 (d, J = 8.4 Hz, 4H), 7.31 (d, J = 8.4 Hz, 4H), 3.40 (s, 6H), 1.55 (s, 36H), 1.53 (s, 36H). HRMS (MALDI-TOF): calcd for $C_{90}H_{105}O_{24}SSi^+$ ([M$^+$]) 1630.6514, found 1630.6504.

General Procedure for the TPSiS Resist Lithography. The TPSiS resist was dissolved in propylene glycol methyl ether acetate (PGMEA) making a 30 mg/mL solution. The solution was filtered through a 0.22 μm membrane filter twice and spin-coated on silicon wafers (2200−2500 rpm, 30 s) to form thin films of 42−48 nm thickness. Each 2 in. silicon wafer was primed by hexamethyl disilazane before coating. A postapplication bake temperature of 100 °C for 180 s was applied to resist film using a hot plate to remove excess casting solvent PGMEA. The film thickness was measured by a spectroscopic ellipsometer, and the film was then exposed by EBL. For the PTD, the exposed film was baked at 70 °C for 30 s, developed with 2.38 wt % tetramethylammonium hydroxide (TMAH) solution, and then rinsed in deionized water before drying. For the NTD, the exposed film was baked at different temperatures (°C) for 30 s and developed with a mixed organic solvent consisting of chlorocyclohexane and n-hexane.

https://doi.org/10.1021/acsomega.2c08112
ACS Omega 2023, 8, 12173−12182

The resulting patterns were inspected using SEM or AFM. The LER and LWR parameters for all the patterns were analyzed by the software ProSEM. All the lines in the image were selected for analysis, and the LER on the left and the right were obtained, respectively. The average value of them was taken as the LER value of the image.

Etching Resistance. An area of 2 × 10 μm^2 rectangular was exposed at a dose of 45 $\mu C/cm^2$ by electron beam and then baked and developed in the optimizing conditions. Standard cryogenic etching is a very stable, reproducible, and clean process, which produces high resist selectivity and high anisotropy without sidewall scalloping.[51] The developed film was etched using a SF_6/O_2 mixture plasma at −110 °C according to the typical temperature.[52] The etching depth was examined by AFM. The residual resist after etching was removed by ultrasonic in acetone and MIBK for 1 min, respectively.

RESULTS AND DISCUSSION

Synthesis and Characterization. The TPSiS was prepared in five steps according to Scheme 1. Each compound was characterized by ^{1}H NMR and HR-MS. The Suzuki−Miyaura coupling reaction between **2** and 3,4-dimethoxyphenylboronic acid was conducted, producing compound **3** in an 87% yield. Treatment of **3** with BBr_3 at 0 °C afforded the corresponding polyhydroxy derivative without any purification. The crude residue was then protected with *t*-Boc groups to get compound **4**. Finally, TPSiS was prepared by the reaction between **4**, silver trifluoromethanesulfonate, and methyl iodide at 0 °C in darkness for 30 min. The ^{1}H NMR spectrum of TPSiS in $CDCl_3$ is depicted in Figure S1. The characteristic signal of the methyl protons on the sulfonium unit of TPSiS was located at 3.40 ppm, indicating the target product of the PAG-bound MG. The peaks at 1.53−1.55 ppm were assigned to the methyl protons in the spectrum of TPSiS, indicating the introduction of the *t*-Boc pendant groups. The formation of TPSiS was further confirmed by the high-resolution MALDI-TOF mass spectrum (Figure S2), giving its ion peak at m/z = 1630.6504 (calcd 1630.6514 [M^+]) for TPSiS.

Physical Properties of the TPSiS. Good thermal stability is a prerequisite for resist's use in patterning formation. The thermal behavior of TPSiS was investigated by TGA and DSC, as shown in Figure 2. TPSiS exhibited a relatively high thermal

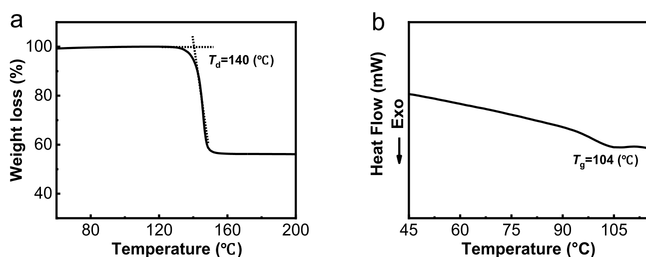

Figure 2. TGA and DSC curves of TPSiS: (a) TGA and (b) DSC.

stability (T_d = 140 °C), and the weight loss corresponded to the weight percentage of *t*-Boc groups of TPSiS, suggesting the decomposition of *t*-Boc groups occurred at around 140 °C. DSC analysis revealed that TPSiS exhibited a T_g around 104 °C. These results confirm that TPSiS is fit for the two bake processes during the lithography.

A homogeneous film is highly desired for patterning. Crystallization is unfavorable to the formation of uniform films. To confirm the amorphous state of TPSiS, the PXRD of TPSiS was measured. It exhibited a broad peak that centered at 2θ = 25° and a weak shoulder (Figure S3a), suggesting TPSiS is amorphous and suitable for spin-coating to form uniform thin films. The amorphous character of TPSiS may be attributed to the nonplanar and tetrahedral structure of Si compounds. The spin-coated TPSiS film was further investigated by atomic force microscope (Figure S3b,c). The surface roughness of the obtained film was 0.34 nm in an area of 5 × 5 μm^2. This indicates that TPSiS is suitable for high-resolution lithography.

The introduction of the sulfonium salt unit will reduce the solubility of the molecule in organic solvents.[27] However, the ionic TPSiS shows good solubility in organic solvents, such as ethyl acetate, THF, and PGMEA. To get an optimal developer, the solubility characteristic of TPSiS thin films in exposed and unexposed regions were examined by electron beam exposure. An area of 5 × 1 mm^2 rectangular was exposed by electron beam, and after baking at 70 °C for 30 s, the resulting films were developed in different solvents. The developed patterns were observed by an optical microscope. The results are summarized in Table 1. Both exposed and unexposed TPSiS

Table 1. Solubility of TPSiS Films before and after Electron Beam Exposure[a]

Solvent	Before exposure	After exposure
PGMEA	+	+
Isopropyl alcohol	+	+
2.38 wt % TMAH aq.	−	+
n-Hexane	+ −	−
Cyclohexane	+ −	−
Chlorocyclohexane	+	−
Toluene	+	−
Anisole	+	+ −

[a]+: Soluble at room temperature; + −: partly soluble; and −: insoluble.

films were soluble in PGMEA and IPA solvents, failing to produce an effective switch of solubility. The TPSiS film solubility switch from insoluble to soluble in 2.38 wt % TMAH aqueous by electron beam exposure suggests a PTD. Conversely, the exposure area became less soluble in chlorocyclohexane, toluene, or anisole upon exposure, demonstrating a NTD. The partial solubility of unexposed TPSiS film in *n*-hexane and cyclohexane makes it possible for tuning the film solubility in a mixed developer by changing the fraction for NTD. The solubility switch of TPSiS film by electron beam exposure in different solvents suggests a dual-tone development via tuning developers.

Photoacid Generation. To confirm the photoacid generation of TPSiS, the solution of TPSiS and the acid-sensitive indicator rhodamine B in THF was irradiated at a wavelength of 254 nm. The absorbance and color changes of the mixture solution at different exposure doses were measured and are shown in Figure 3. With the increase of exposure doses (0−230 mJ/cm^2), the absorption intensity at 556 nm, which was assigned to the protonated rhodamine B, increased obviously (Figure 3a). The color of the corresponding solution turned from colorless to pink and rose red gradually (Figure 3b). The acid generation efficiency of the TPSiS molecule in

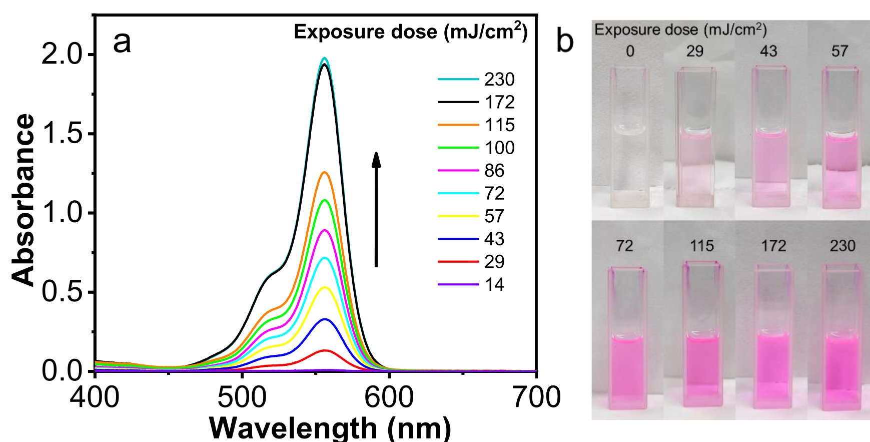

Figure 3. Evolution of mixture solution of RB and TPSiS exposed to 254 nm light with different exposure doses: (a) UV absorbance; and (b) color change to the naked eye.

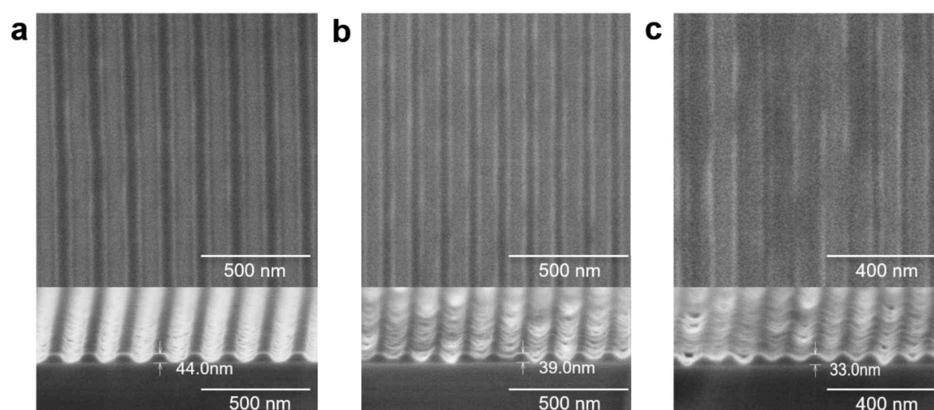

Figure 4. Top-down view (top) and corresponding cross-sectional view (bottom) of different patterns under a dose of 200 μC/cm^2: (a) HP 80 nm, (b) HP 60 nm, and (c) HP 50 nm. The film thickness was 44 nm.

Table 2. Lithographic Evaluation Data of the TPSiS Resist Developed in Different Organic Developers[a]

Organic developer (chlorocyclohexane/*n*-hexane)[b]	Dose[c] (μC/cm^2)	LER (nm)	Pattern[d]	Patterning capability
1:3	–	–	no	no
1:2	40	5.7	Figure S6, red frame	good
1:1	50	6.5	Figure S6, green frame	poor
3:1	80	7.3	Figure S6, blue frame	poor
1:0	100	9.2	Figure S6, purple frame	very poor

[a]Calculated from HP 30 nm patterns. [b]Volume ratio. [c]Dose of forming 1:1 line/space patterns at the pitch of 60 nm. [d]PEB at 70 °C for 30 s on a 42 nm resist film.

THF solution is estimated to be 0.05 with the irradiation of 254 nm light by using rhodamine B as an indicator.[53] It demonstrates that the TPSiS can generate acid continuously with the irradiation of UV light. Previous studies have demonstrated that photolysis of the sulfonium salt to sulfides results in acid.[54,55] To further confirm the reaction, the ^{1}H NMR spectra of the irradiated TPSiS solution at 254 nm in chloroform-*d* were performed. A new signal at 2.49 ppm was observed, which agrees with the protons of methyl in phenyl methyl sulfide of compound 4 (Figure S4). It shows that the sulfonium salt unit undergoes decomposition. FT-IR spectra of the TPSiS film on wafers (~300 nm) before and after exposure to 254 nm light were measured. A broad new peak at 3374 cm^{-1} appeared on the IR spectra, confirming the deprotection of *t*-Boc groups and the formation of hydroxyl (Figure S5). All the results demonstrate that the generation of photoacid and the acid-catalyzed deprotection occurred simultaneously in TPSiS film, suggesting the potential of TPSiS to be used as a single-component resist.

Patterning Properties of the TPSiS Resist in EBL. The lithographic performance of the TPSiS resist was investigated for PTD via a 100 kV electron beam system. The preparation of the resist and the films could be found in the Experimental Section. Figure 4 shows the typical SEM configurations developed in a standard TMAH aqueous solution (2.38 wt %) with half-pitches (HPs) of 80, 60, and 50 nm layouts for the TPSiS resist. HP 80 and 60 nm patterns were almost achieved from the top-view but failed to give HP 50 nm pattern due to the residues of the resist. The corresponding cross-sectional images demonstrated an obvious footing phenomenon in the HP 80 pattern (Figure 4a). A higher degree of resist residues in the trench was observed in the

https://doi.org/10.1021/acsomega.2c08112
ACS Omega 2023, 8, 12173−12182

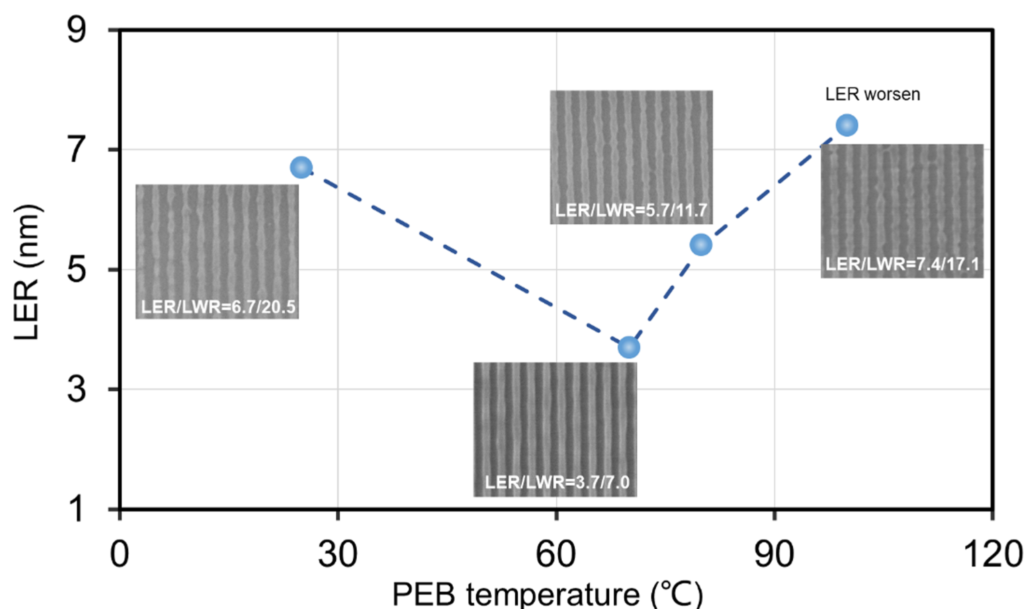

Figure 5. LER and LWR values at different PEB temperatures, together with corresponding HP 30 nm patterns for the TPSiS resist at an exposure dose of 40 $\mu C/cm^2$. The PEB time was set at 30 s.

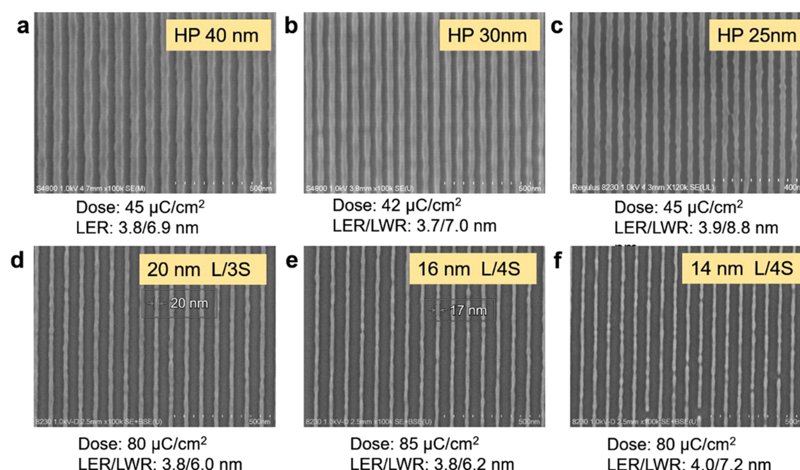

Figure 6. SEM images of the dense lines/space patterns with half-pitches of (a) 40, (b) 30, and (c) 25 nm and semidense line/space patterns of (d) 20 nm L/3S, (e) 16 nm L/4S, and (f) 14 nm L/4S.

higher resolution patterns (Figure 4b,c). We speculate that a more hydrophobic thioether unit after exposure makes the exposed region insoluble in TMAH solution, leading to incomplete development. It suggests that the TPSiS resist is unfavorable to giving high-resolution patterns for PTD.

The preliminary solubility studies indicated that organic solvents could be used as developers for TPSiS resist in NTD. Chlorocyclohexane exhibited a better ability to dissolve TPSiS than hexane. To get the best developing conditions for NTD, the mixtures with different ratios of chlorocyclohexane to hexane were used for the development process. The lithographic performances of the TPSiS resist in different organic developers by EBL were evaluated as shown in Figure S6. The TPSiS resist shows different optimal exposure doses in different developers. The results for 30 nm HP patterns are summarized in Table 2. The exposure doses of the TPSiS resist increase as the volume ratio of chlorocyclohexane increases. It is attributed to the increase of the solubility of the developers for unexposed areas, and higher doses are required for the formation of negative patterns. The quality of the lithographic pattern was strongly correlated with the volume ratios of chlorocyclohexane in organic developers. No pattern was observed after developing by a 1:3 chlorocyclohexane/hexane mixture because of weak developing ability. Increasing the volume ratio of chlorocyclohexane/hexane from 1:3 to 1:2, a clear pattern without pinching or fracture was observed (Figure S6, red frame). Continuing to increase the proportion of chlorocyclohexane, the lithographic patterns become worse, giving larger LER values ranging from 6.5 to 9.2 nm (Table 2, Figure S6). These results confirm that the hexane/chlorocyclohexane mixture in a 2:1 ratio is an optimal developer for TPSiS resist.

To optimize the PEB process and obtain high-resolution lithographic patterns, the EBL performance of TPSiS resist at different PEB temperatures was investigated by measuring the LER and LWR values of line patterns. Layout with HP 30 nm was exposed at a dose of 40 $\mu C/cm^2$. After exposure, the samples were baked at 25, 70, 80, and 100 °C for 30 s,

https://doi.org/10.1021/acsomega.2c08112
ACS Omega 2023, 8, 12173−12182

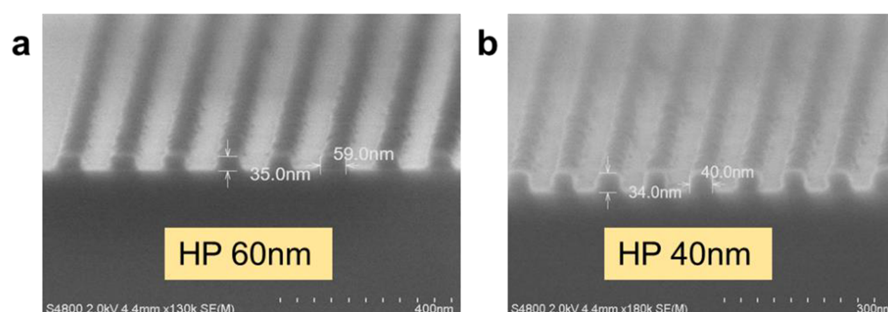

Figure 7. Cross-section patterns of (a) HP 60 nm and (b) HP 40 nm for the TPSiS resist (film thickness: 48 nm).

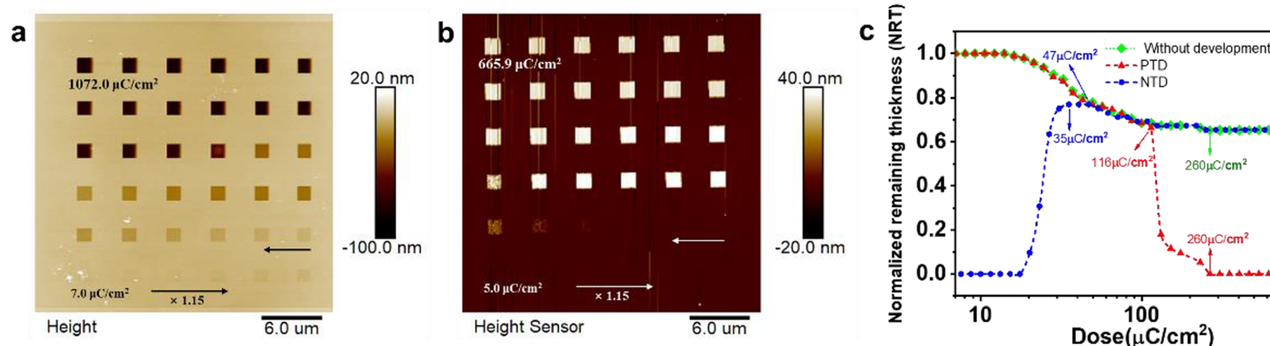

Figure 8. AFM images of TPSiS resist pattern blocks developed with (a) 2.38 wt % TMAH solution and (b) the mixture of hexane/chlorocyclohexane (2:1). (c) Contrast curves of the TPSiS resist developed by 2.38 wt % TMAH solution, hexane-chlorocyclohexane (2:1) mixture solvent, and without development.

respectively, and then they were developed in hexane/chlorocyclohexane (2:1) mixture for 30 s. The lithographic HP 30 nm patterns under various PEB temperatures together with the LER values were figured in Figure 5. In the case of PEB at room temperature of 25 °C, an obvious necking was observed, giving a high LER value of 6.7 nm. It is attributed to the insufficient acid-catalyzed deprotection of *t*-Boc groups at a low PEB temperature.[56] Increasing PEB temperature to 70 °C, the patterns became clear and the LER decreased to 3.7 nm, suggesting a proper PEB temperature could make the deprotection reaction sufficient and homogeneous, which reduced the LER value. At higher PEB temperatures above 70 °C, the LER values of the patterns gradually became larger. It is attributed to the excessive diffusion of photoacid from the exposed to unexposed regions at high PEB temperature, which induced the bridging and a continuous increase of LER value in NTD patterns.[57,58] The results confirm that 70 °C is an optimal PEB temperature for the TPSiS resist in EBL performance.

The capability of forming 1:1 line/space patterns of the TPSiS resist was further examined under the optimum PEB and developing conditions. The typical HP 40, 30, and 25 nm dense line patterns were achieved at the dose of 42−45 $\mu C/cm^2$ as shown in Figure 6a−c. As an example, the LER and LWR parameters for HP 25 nm pattern calculated by ProSEM software are shown in Figure S7. The lithographic patterns exhibited high contrast and a low LER (≤3.9 nm). Additionally, features such as 20 nm L/3S and 16 nm L/4S lines were also achieved at a dose of 80 and 85 $\mu C/cm^2$, as shown in Figure 6d,e. The measured line width was consistent with the default features of layouts, which indicates that the TPSiS resist is capable of forming patterns accurately. In the case of the smaller feature size of 14 nm L/4S, an obvious pinching was observed (Figure 6f), which resulted in a higher LER (5.3 nm). For comparison, the performance of TPSiS resist, some newly reported CARs, and the commercially available EB resists are summarized in Table S1. The sensitivity of the TPSiS resist is higher than that of most resists. Compared with negative-tone CAR of SU-8 resist, the TPSiS resist simultaneously improves the resolution (34 vs 25 nm) and LER value (6.0 vs 3.9 nm) of lithographic patterns while maintaining high sensitivity. The results suggest that the TPSiS resist has the potential to be applied in nanofabrication as EBL resist materials with high resolution and sensitivity.

To evaluate the pattern profile of the TPSiS resist via NTD, the cross-section SEM images of lithographic patterns were measured, as shown in Figure 7. These lithographic stripes had good vertical profiles. No footing was observed in the space areas. Notably, there was no residue in the trench, which was significantly different from the PTD patterns (Figure 4) and confirmed a clean development. The line width and period measured from the cross-section images (Figure 7b) were in complete agreement with the results from the top-view (Figure 6a), suggesting the TPSiS resist is capable of forming patterns accurately. It should be noted that the height of the stripes was 34.0 nm, which was smaller than the film thickness (48.0 nm), indicating a loss of resist film. This may attribute to the volume contraction of residual resist after the deprotection of *t*-Boc groups during exposure and PEB processes.

The etching resistance is an important factor for photoresists to accurately transfer patterns. The etching rate of the TPSiS resist films after NTD was measured by using a SF_6/O_2 mixture plasma (Experimental Section). Figure S9 shows the three-dimensional AFM topography images of the exposed TPSiS resist after etching (Figure S9a) and resist-strip (Figure S9b), together with their corresponding sections and height

values. The height of TPSiS resist film was 37.0 nm before etching (measured by SEM). The remaining resist thickness was 9.0 nm calculated by comparing the height difference before and after stripping. The etching depths of the TPSiS resist and Si substrate were 28 and 240 nm in 10 s, giving etching rates of 2.8 and 24 nm/s, respectively. The etching selectivity of the TPSiS resist to the silicon substrate was 8.6:1, indicating an excellent pattern transfer property.

Contrast Analysis. To investigate the patterning behavior of the TPSiS resist in different developers, the contrast curves of the TPSiS resist developed in 2.38 wt % TMAH solution or hexane/chlorocyclohexane (2:1) mixture were measured. The resist films were exposed on several squares ($1.5 \times 1.5\ \mu m^2$) with varying doses. After baking and developing, the remaining thickness in each exposure square was measured by AFM (Figure 8). Figure 8a,b shows the AFM images of TPSiS resist pattern blocks developed in 2.38 wt % TMAH solution and hexane/chlorocyclohexane (2:1) mixture, respectively. As a comparison, the contrast of the TPSiS resist without development was also measured. The contrast curves of the TPSiS resist are shown in Figure 8c. In the case of PTD, the dark loss of TPSiS resist film in TMAH (2.38%) aqueous developer is almost negligible. A two-stage decrease of the normalized remaining thickness (NRT) was observed. This was a stage of slow decrease below the dose of 116 $\mu C/cm^2$ and a stage of dramatically decreased at a dose range of 116 to 260 $\mu C/cm^2$, giving a low contrast of 0.8 (Supporting Information). The slow stage almost overlapped with the curves of the process without development, suggesting a poor solubility of the partial deprotecting product in TMAH solution. It means a high ratio of deprotection is required to switch the solubility, which is much higher than the typical PTD resists (ranging from 50 to 75%).[59] The inefficient switch of the solubility results in a low contrast of the TPSiS resist, which is consistent with the footing in the HP 80 and 60 nm patterns by PTD. In contrast, the NRT drastically increased within the dose range of 18−35 $\mu C/cm^2$ for NTD, giving a higher contrast (γ = 3.4). The NTD curve and the curve without development were completely coincident above 47 $\mu C/cm^2$, suggesting that the fully irradiated TPSiS resist film was completely insoluble in the organic developer. A significant solubility switch is achieved within a narrow exposure dose range (18−47 $\mu C/cm^2$), which was favorable to obtaining high-resolution patterns by NTD. The dark loss in NTD was about 30% estimated by the final remaining thickness (70%), which is consistent with results from the ratio of the cross-section pattern height (34 nm) to film thickness (48 nm) (Figure 7). The loss of the resist film maybe comes from the volume contraction of the partial decomposition of *t*-Boc groups and the sulfonium salt.[50]

■ CONCLUSION

In summary, a novel PAG-bound MG resist (TPSiS) was synthesized and characterized. TPSiS showed good thermal stability and film-forming ability. It could be used as a single-component chemically amplified molecular resist without any additives. It failed to achieve high-resolution patterns by PTD in TMAH solution due to the unclean development. However, by optimizing the process conditions, the TPSiS resist could resolve 25 nm dense line/space patterns and 16 nm L/4S semidense line/space patterns at a dose of 45 and 85 $\mu C/cm^2$ by NTD. Contrast analysis revealed that the significant solubility switch within a narrow exposure dose range by NTD played an important role in the formation of high-resolution patterns. This study supplies useful guidelines for the optimization and development of single-component MG resists with high lithographic performance.

■ ASSOCIATED CONTENT

Supporting Information

The Supporting Information is available free of charge at https://pubs.acs.org/doi/10.1021/acsomega.2c08112.

NMR and MS spectra, roughness measurement of film by AFM analysis, Fourier-transform infrared spectroscopy data, SEM images, summary of commercially available EB resists, etch selectivity measurement of resist, and the method of contrast calculation (PDF)

■ AUTHOR INFORMATION

Corresponding Authors

Jinping Chen − *Key Laboratory of Photochemical Conversion and Optoelectronic Materials, Technical Institute of Physics and Chemistry, Chinese Academy of Sciences, Beijing 100190, China;* orcid.org/0000-0002-5632-2290; Email: chenjp@mail.ipc.ac.cn

Yi Li − *Key Laboratory of Photochemical Conversion and Optoelectronic Materials, Technical Institute of Physics and Chemistry, Chinese Academy of Sciences, Beijing 100190, China; University of Chinese Academy of Sciences, Beijing 100049, China;* orcid.org/0000-0002-7018-180X; Email: yili@mail.ipc.ac.cn

Guoqiang Yang − *Beijing National Laboratory for Molecular Sciences (BNLMS), Key Laboratory of Photochemistry, Institute of Chemistry, Chinese Academy of Sciences, Beijing 100190, China; University of Chinese Academy of Sciences, Beijing 100049, China;* orcid.org/0000-0003-0726-2217; Email: gqyang@iccas.ac.cn

Authors

Yake Wang − *Key Laboratory of Photochemical Conversion and Optoelectronic Materials, Technical Institute of Physics and Chemistry, Chinese Academy of Sciences, Beijing 100190, China; University of Chinese Academy of Sciences, Beijing 100049, China*

Jundi Yuan − *Key Laboratory of Photochemical Conversion and Optoelectronic Materials, Technical Institute of Physics and Chemistry, Chinese Academy of Sciences, Beijing 100190, China; University of Chinese Academy of Sciences, Beijing 100049, China*

Yi Zeng − *Key Laboratory of Photochemical Conversion and Optoelectronic Materials, Technical Institute of Physics and Chemistry, Chinese Academy of Sciences, Beijing 100190, China; University of Chinese Academy of Sciences, Beijing 100049, China;* orcid.org/0000-0003-0694-1795

Tianjun Yu − *Key Laboratory of Photochemical Conversion and Optoelectronic Materials, Technical Institute of Physics and Chemistry, Chinese Academy of Sciences, Beijing 100190, China;* orcid.org/0000-0003-2064-3655

Xudong Guo − *Beijing National Laboratory for Molecular Sciences (BNLMS), Key Laboratory of Photochemistry, Institute of Chemistry, Chinese Academy of Sciences, Beijing 100190, China;* orcid.org/0000-0002-2012-4399

Shuangqing Wang − *Beijing National Laboratory for Molecular Sciences (BNLMS), Key Laboratory of Photochemistry, Institute of Chemistry, Chinese Academy of*

Sciences, Beijing 100190, China; orcid.org/0000-0002-8281-9399

Complete contact information is available at:
https://pubs.acs.org/10.1021/acsomega.2c08112

Notes

The authors declare no competing financial interest.

■ ACKNOWLEDGMENTS

This work was supported by the National Natural Science Foundation of China (22090012, U20A20144). The Foundation of Technical Institute of Physics and Chemistry (TIPC) Chinese Academy of Sciences (CAS) is gratefully acknowledged. We also thank the National Center for Nanoscience and Technology for EBL and etching experiments.

■ REFERENCES

(1) Schwierz, F.; Pezoldt, J.; Granzner, R. Two-dimensional materials and their prospects in transistor electronics. *Nanoscale* **2015**, *7* (18), 8261−8283.

(2) Golio, M. Fifty years of moore's law. *Proc. IEEE* **2015**, *103* (10), 1932−1937.

(3) Miyazaki, J.; Yen, A. EUV Lithography Technology for High-volume Production of Semiconductor Devices. *J. Photopolym Sci. Technol.* **2019**, *32* (2), 195−201.

(4) Luo, S. H.; Hoff, B. H.; Maier, S. A.; de Mello, J. C. Scalable Fabrication of Metallic Nanogaps at the Sub-10 nm Level. *Adv. Sci.* **2021**, *8* (24), 2102756.

(5) Peng, X. M.; Wang, Y. F.; Xu, J.; Yuan, H.; Wang, L. Q.; Zhang, T.; Guo, X. D.; Wang, S. Q.; Li, Y.; Yang, G. Q. Molecular Glass Photoresists with High Resolution, Low LER, and High Sensitivity for EUV Lithography. *Macromol. Mater. Eng.* **2018**, *303* (6), 1700654.

(6) Li, L.; Liu, X.; Pal, S.; Wang, S. L.; Ober, C. K.; Giannelis, E. P. Extreme ultraviolet resist materials for sub-7 nm patterning. *Chem. Soc. Rev.* **2017**, *46* (16), 4855−4866.

(7) Manouras, T.; Argitis, P. High Sensitivity Resists for EUV Lithography: A Review of Material Design Strategies and Performance Results. *Nanomaterials* **2020**, *10* (8), 1593.

(8) Woodward, J. T.; Hwang, J.; Prabhu, V. M.; Choi, K. W. Hunting the origins of line width roughness with chemical force microscopy. *Proc. SPIE* **2007**, *931*, 413−418.

(9) Lawson, R. A.; Henderson, C. L. Mesoscale simulation of molecular resists: The effect of PAG distribution homogeneity on LER. *Microelectron. Eng.* **2009**, *86*, 741−744.

(10) Lawson, R. A.; Henderson, C. L. Mesoscale kinetic Monte Carlo simulations of molecular resists: effects of photoacid homogeneity on resolution, line-edge roughness, and sensitivity. *J. Micro/Nanolithogr. MEMS, MOEMS* **2010**, *9* (1), 013016.

(11) Jablonski, E. L.; Prabhu, V. M.; Sambasivan, S.; Fischer, D. A.; Lin, E. K.; Goldfarb, D. L.; Angelopoulos, M.; Ito, H. Surface and bulk chemistry of chemically amplified photoresists: segregation in thin films and environmental stability issues. *Proc. SPIE* **2004**, *5376*, 302−311.

(12) Green, D. P.; Jain, V.; Bailey, B.; Wagner, M.; Clark, M.; Valeri, D.; Lakso, S. Development of Molecular Resist Derivatives for EUV Lithography. *Proc. SPIE* **2013**, *8679*, 867912.

(13) Irie, M.; Suzuki, T.; Mimura, T.; Iwai, T. Resist development to improve flare issue for EUV lithography. *Proc. SPIE* **2008**, *6923*, 92310.

(14) Lu, X. Y.; Luo, H.; Wang, K.; Zhang, Y. Y.; Zhu, X. F.; Li, D. X.; Ma, B. Z.; Xiong, S. S.; Nealey, P. F.; Li, Q.; Wu, G. P. CO_2-Based Dual-Tone Resists for Electron Beam Lithography. *Adv. Funct. Mater.* **2021**, *31* (13), 2007417.

(15) Liao, P. C.; Chen, P. H.; Tseng, Y. F.; Shih, T. A.; Lin, T. A.; Gau, T. S.; Lin, B. J.; Chiu, P. W.; Liu, J. H. Partial decarboxylation of hafnium oxide clusters for high resolution lithographic applications. *J. Mater. Chem. C* **2022**, *10* (41), 15647−15655.

(16) Yi, X. F.; Wang, D.; Li, F.; Zhang, J.; Zhang, L. Molecular bixbyite-like In_{12}-oxo clusters with tunable functionalization sites for lithography patterning applications. *Chem. Sci.* **2021**, *12* (43), 14414−14419.

(17) Nandi, S.; Khillare, L.; Moinuddin, M. G.; Kumar, S.; Chauhan, M.; Sharma, S. K.; Ghosh, S.; Gonsalves, K. E. Macrocycle Network-Aided Nanopatterning of Inorganic Resists on Silicon. *ACS Appl. Nano Mater.* **2022**, *5* (8), 10268−10279.

(18) Miao, Y. R.; Tsapatsis, M. Electron Beam Patterning of Metal-Organic Frameworks. *Chem. Mater.* **2021**, *33* (2), 754−760.

(19) Shi, J.; Ravi, A.; Richey, N. E.; Gong, H.; Bent, S. F. Molecular Layer Deposition of a Hafnium-Based Hybrid Thin Film as an Electron Beam Resist. *ACS Appl. Mater. Interfaces* **2022**, *14* (23), 27140−27148.

(20) Yang, D. X.; Chen, X. Y.; He, D. S.; Frommhold, A.; Shi, X. Q.; Boden, S. A.; Lebedeva, M. A.; Ershova, O. V.; Palmer, R. E.; Li, Z. Y.; Shi, H. F.; Gao, J. Z.; Pan, M. H.; Khlobystov, A. N.; Chamberlain, T. W.; Robinson, A. P. G. A Fullerene-Platinum Complex for Direct Functional Patterning of Single Metal Atom-Embedded Carbon Nanostructures. *J. Phys. Chem. Lett.* **2022**, *13* (6), 1578−1586.

(21) Saifullah, M. S. M.; Asbahi, M.; Neo, D. C. J.; Mahfoud, Z.; Tan, H. R.; Ha, S. T.; Dwivedi, N.; Dutta, T.; bin Dolmanan, S.; Aabdin, Z.; Bosman, M.; Ganesan, R.; Tripathy, S.; Hasko, D. G.; Valiyaveettil, S. Patterning at the Resolution Limit of Commercial Electron Beam Lithography. *Nano Lett.* **2022**, *22* (18), 7432−7440.

(22) Yogesh, M.; Moinuddin, M. G.; Chauhan, M.; Sharma, S. K.; Ghosh, S.; Gonsalves, K. E. Organoiodine Functionality Bearing Resists for Electron-Beam and Helium Ion Beam Lithography: Complex and Sub-16 nm Patterning. *ACS Appl. Electron. Mater.* **2021**, *3* (5), 1996−2004.

(23) Wang, Z.; Chen, J.; Yu, T.; Zeng, Y.; Guo, X.; Wang, S.; Allenet, T.; Vockenhuber, M.; Ekinci, Y.; Yang, G.; Li, Y. Sulfonium-Functionalized Polystyrene-Based Nonchemically Amplified Resists Enabling Sub-13 nm Nanolithography. *ACS Appl. Mater. Interfaces* **2023**, *15* (1), 2289−2300.

(24) Gonsalves, K. E.; Thiyagarajan, M.; Dean, K. New resists for nanometer scale patterning by extreme ultraviolet lithography. *J. Microlith. Microfab, Microsyst.* **2005**, *4* (2), 029701.

(25) Lee, C. T.; Henderson, C. L.; Wang, M. X.; Gonsalves, K. E.; Yueh, W. Effects of photoacid generator incorporation into the polymer main chain on 193 nm chemically amplified resist behavior and lithographic performance. *J. Vac. Sci. Technol. B* **2007**, *25* (6), 2136−2139.

(26) Wang, M. X.; Gonsalves, K. E.; Rabinovich, M.; Yueh, W.; Roberts, J. M. Novel anionic photoacid generators (PAGs) and corresponding PAG bound polymers for sub-50 nm EUV lithography. *J. Mater. Chem.* **2007**, *17* (17), 1699−1706.

(27) Wang, Q. Q.; Yan, C. F.; You, F. J.; Wang, L. Y. A new type of sulfonium salt copolymers generating polymeric photoacid: Preparation, properties and application. *React. Funct. Polym.* **2018**, *130*, 118−125.

(28) Wang, Q. Q.; Zhang, C. Y.; Yan, C. F.; You, F. J.; Wang, L. Y. One-component chemically amplified resist composed of polymeric sulfonium salt PAGs for high resolution patterning. *Eur. Polym. J.* **2019**, *114*, 11−18.

(29) Yoo, J. B.; Park, S. W.; Kang, H. N.; Mondkar, H. S.; Sohn, K.; Kim, H. M.; Kim, K. B.; Lee, H. Triphenylsulfonium salt methacrylate bound polymer resist for electron beam lithography. *Polymer* **2014**, *55* (16), 3599−3604.

(30) Wu, H. P.; Gonsalves, K. E. Preparation of a photoacid generating monomer and its application in lithography. *Adv. Funct. Mater.* **2001**, *11* (4), 271−276.

(31) Yogesh, M.; Moinuddin, M. G.; Khillare, L. D.; Chinthalapalli, S.; Sharma, S. K.; Ghosh, S.; Gonsalves, K. E. Organotin bearing polymeric resists for electron beam lithography. *Microelectron. Eng.* **2022**, *260*, 111795.

(32) Tarutani, S.; Tamaoki, H.; Tsubaki, H.; Takahashi, T.; Takizawa, H.; Takahashi, H. Characterizing Polymer bound PAG Type EUV Resist. *J. Photopolym. Sci. Technol.* **2011**, *24* (2), 185−191.

(33) Allen, R. D.; Brock, P. J.; Na, Y. H.; Sherwood, M. H.; Truong, H. D.; Wallraff, G. M.; Fujiwara, M.; Maeda, K. Investigation of Polymer-bound PAGs: Synthesis, Characterization and Initial Structure/Property Relationships of Anion-bound Resists. *J. Photopolym. Sci. Technol.* **2009**, *22* (1), 25−29.

(34) Yamamoto, H.; Kozawa, T.; Tagawa, S. Study on dissolution behavior of polymer-bound and polymer-blended photo acid generator (PAG) resists by using quartz crystal microbalance (QCM) method. *Microelectron. Eng.* **2014**, *129*, 65−69.

(35) Hirayama, T.; Kim, S. M.; Na, H. S.; Koh, C.; Kim, H. W. Limitation of blend type of resist platform on EUV lithography. *Proc. SPIE* **2012**, *8325*, 83251D.

(36) Wu, H. P.; Gonsalves, K. E. Novel positive-tone chemically amplified resists with photoacid generator in the polymer chains. *Adv. Mater.* **2001**, *13* (9), 670−672.

(37) Wu, H. P.; Gonsalves, K. E. A novel single-component negative resist for DUV and electron beam lithography. *Adv. Mater.* **2001**, *13* (3), 195−197.

(38) Lee, C. T.; Henderson, C. L.; Wang, M. X.; Gonsalves, K. E.; Yueh, W.; Roberts, J. M. The effect of direct PAG incorporation into the polymer main chain on reactive ion etch resistance of 193 nm and EUV chemically amplified resists. *Microelectron. Eng.* **2008**, *85*, 963−965.

(39) De Silva, A.; Felix, N. M.; Ober, C. K. Molecular glass resists as high-resolution patterning materials. *Adv. Mater.* **2008**, *20* (17), 3355−3361.

(40) Dai, J. Y.; Chang, S. W.; Hamad, A.; Yang, D.; Felix, N.; Ober, C. K. Molecular glass resists for high-resolution patterning. *Chem. Mater.* **2006**, *18* (15), 3404−3411.

(41) Nishikubo, T.; Kudo, H. Recent Development in Molecular Resists for Extreme Ultraviolet Lithography. *J. Photopolym Sci. Technol.* **2011**, *24* (1), 9−18.

(42) Chen, J. P.; Hao, Q. S.; Wang, S. Q.; Li, S. Y.; Yu, T. J.; Zeng, Y.; Zhao, J.; Yang, S. M.; Wu, Y. Q.; Xue, C. F.; Yang, G. Q.; Li, Y. Molecular Glass Resists Based on 9,9'-Spirobifluorene Derivatives: Pendant Effect and Comprehensive Evaluation in Extreme Ultraviolet Lithography. *ACS Appl. Polym. Mater.* **2019**, *1* (3), 526−534.

(43) Hu, S. W.; Chen, J. P.; Yu, T. J.; Zeng, Y.; Yang, G. Q.; Li, Y. Chemically Amplified Resist Based on Dendritic Molecular Glass for Electron Beam Lithography. *Chem. Res. Chin. Univ.* **2023**, *39* (1), 139−143.

(44) Kasai, T.; Higashihara, T.; Ueda, M. A novel photo-acid generator bound molecular glass resist with a single protecting group. *J. Polym. Sci., Polym. Chem.* **2013**, *51* (9), 1956−1962.

(45) Lawson, R. A.; Tolbert, L. M.; Henderson, C. L. Single-component molecular resists containing bound photoacid generator functionality. *J. Micro/Nanolithogr., MEMS, MOEMS* **2010**, *9* (1), 013015.

(46) Oizumi, H.; Matsunaga, K.; Kaneyama, K.; Santillan, J. J.; Shiraishi, G.; Itani, T. Performance of EUV molecular resists based on fullerene derivatives. *Proc. SPIE* **2011**, *7972*, 797209.

(47) Lawson, R. A.; Lee, C. T.; Tolbert, L. M.; Henderson, C. L. Effect of acid anion on the behavior of single component molecular resists incorporating ionic photoacid generators. *Microelectron. Eng.* **2009**, *86* (4−6), 738−740.

(48) Sobarzo, P. A.; Jessop, I. A.; Mariman, A. P.; Gonzalez, A. F.; Saldías, C.; Schott, E.; Zarate, X.; Hauyon, R. A.; Recabarren-Gajardo, G.; González-Henríquez, C. M.; Tundidor-Camba, A.; Terraza, C. A. New thiophene-based poly(azomethine)s bearing tetraphenylsilane moieties along their backbone. Optical, electronic, thermal properties and theoretical calculations. *Eur. Polym. J.* **2020**, *130*, 109658.

(49) Wang, Y.; Chen, J.; Zeng, Y.; Yu, T.; Guo, X.; Wang, S.; Allenet, T.; Vockenhuber, M.; Ekinci, Y.; Zhao, J.; Yang, S.; Wu, Y.; Yang, G.; Li, Y. Molecular Glass Resists Based on Tetraphenylsilane Derivatives: Effect of Protecting Ratios on Advanced Lithography. *ACS Omega* **2022**, *7* (33), 29266−29273.

(50) Hu, S. W.; Chen, J. P.; Yu, T. J.; Zeng, Y.; Wang, S. Q.; Guo, X. D.; Yang, G. Q.; Li, Y. A novel dual-tone molecular glass resist based on adamantane derivatives for electron beam lithography. *J. Mater. Chem. C* **2022**, *10* (26), 9858−9866.

(51) Liu, Z. W.; Wu, Y.; Harteneck, B.; Olynick, D. Super-selective cryogenic etching for sub-10 nm features. *Nanotechnology* **2013**, *24*, 015305.

(52) Dussart, R.; Tillocher, T.; Lefaucheux, P.; Boufnichel, M. Plasma cryogenic etching of silicon: from the early days to today's advanced technologies. *J. Phys. D: Appl. Phys.* **2014**, *47* (12), 123001.

(53) Pohlers, G.; Scaiano, J. C.; Sinta, R. A novel photometric method for the determination of photoacid generation efficiencies using benzothiazole and xanthene dyes as acid sensors. *Chem. Mater.* **1997**, *9* (12), 3222−3230.

(54) Dektar, J. L.; Hacker, N. P. Photochemistry of triarylsulfonium salts. *J. Am. Chem. Soc.* **1990**, *112* (16), 6004−6015.

(55) Belmonte, G. K.; da Silva Moura, C. A.; Reddy, P. G.; Gonsalves, K. E.; Weibel, D. E. EUV photofragmentation and oxidation of a polyarylene-Sulfonium resist: XPS and NEXAFS study. *J. Photochem. Photobiol. A: Chem.* **2018**, *364*, 373−381.

(56) Lavery, K. A.; Choi, K. W.; Vogt, B. D.; Prabhu, V. M.; Lin, E. K.; Wu, W. L.; Satija, S. K.; Leeson, M. J.; Cao, H. B.; Thompson, G.; Deng, H.; Fryer, D. S. Fundamentals of the reaction-diffusion process in model EUV photoresists. *Proc. SPIE* **2006**, *6153*, 615313.

(57) Vesters, Y.; De Simone, D.; De Gendt, S. Influence of post exposure bake time on EUV photoresist RLS trade-off. *Proc. SPIE* **2017**, *10143*, 1014324.

(58) Rodríguez-Cantó, P. J.; Nickel, U.; Abargues, R. Understanding Acid Reaction and Diffusion in Chemically Amplified Photoresists: An Approach at the Molecular Level. *J. Phys. Chem. C* **2011**, *115* (42), 20367−20374.

(59) Reilly, M.; Andes, C.; Cardolaccia, T.; Kim, Y. S.; Park, J. K. Evolution of negative tone development photoresists for ArF lithography. *Proc. SPIE* **2012**, *8325*, 832507.